Journal of Physics and Chemistry of Solids 113 (2018) 5–10

Contents lists available at ScienceDirect

Journal of Physics and Chemistry of Solids

journal homepage: www.elsevier.com/locate/jpcs

EDTA-functionalized Fe_3O_4 nanoparticles

A.G. Magdalena [a,*], I.M.B. Silva [a], R.F.C. Marques [b], A.R.F. Pipi [c], P.N. Lisboa-Filho [d], M. Jafelicci Jr. [b]

[a] Department of Chemistry, School of Sciences, São Paulo State University (UNESP), Campus of Bauru, Bauru, São Paulo, Brazil
[b] Department of Physical and Chemistry, Institute of Chemistry, São Paulo State University (UNESP), Campus of Araraquara, Araraquara, São Paulo, Brazil
[c] Associate Dean's Office of Graduate Research (PRPPG), Sagrado Coração University (USC), Bauru, São Paulo, Brazil
[d] Department of Physics, School of Sciences, São Paulo State University (UNESP), Campus of Bauru, Bauru, São Paulo, Brazil

ARTICLE INFO

Keywords:
Magnetite
EDTA
Magnetic nanoparticles
Functionalization

ABSTRACT

This study analyzes the synthesis and characterization of functionalized Fe_3O_4 nanoparticles by ethylenediaminetetraacetic acid (EDTA). The syntheses were performed using the co-precipitation method under different experimental conditions: nitrogen atmosphere versus ambient atmospheric conditions, and temperatures of 25 °C versus 90 °C. X-ray diffraction techniques, Fourier transform infrared (FTIR) spectroscopy, zeta potential, and transmission electron microscopy (TEM) were used to characterize these nanoparticles. The co-precipitation method produced high homogeneity in nanostructure shape and size. The functionalization of the magnetite surface was confirmed by the FTIR analyses and the development of new bands associated with EDTA as well as by zeta potential change. The addition of EDTA was also found to change the mechanism of nucleation and nanostructure growth; EDTA was found to favor nucleation, thus decreasing nanoparticle size.

1. Introduction

Iron oxide nanoparticles are the most commonly used today types of nanostructured system, which exhibit magnetic properties. Iron oxide nanoparticles have also been used in hyperthermia and theranostic devices, a usage which has increased substantially in the last ten years [1–3].

The most frequently studied nanoparticles are iron-based nanoparticles, which are known as nanoscaled zero valent iron (nZVI), maghemite nanoparticles (γ-Fe_2O_3) and magnetite nanoparticles (Fe_3O_4) due to their proven biocompatibilities [1,2,4–6]. These iron-based nanoparticles exhibit unique chemical properties resulting from different iron oxidation states. They are widely used as catalysts in environmental remediation, and as drug delivery vehicles in biomedicine [7]. Interest in nanoparticles has increased in part because they are simple to prepare and are chemically stable when stored in colloidal suspension form. Colloidal suspensions of stabilized magnetic nanoparticles are referred to as ferrofluids and may interact with a external magnetic field [8]. Fe_3O_4 nanoparticles possess the ability to adsorb heavy metals in an aqueous medium through physical and chemical interactions with these heavy metals [7]. However, the major mechanism of contaminant removal from an aqueous medium that employs γ-Fe_2O_3 nanoparticles is physical adsorption [7].

One inevitable problem associated with these particles in this size range is their long-term instability. These particles tend to pursue agglomerates to reduce the energy associated with the increased surface-area-to-volume ratio of nanoparticles. Furthermore, the nanoparticles are chemically very active and easily oxidizes in the air, which generally results in low magnetic properties and dispersibility. For many applications, it is crucial to develop chemical and colloidal protection strategies to chemically stabilize magnetic nanoparticles against degradation during and after synthesis as well as colloidal stability through electrostatical and/or stericstabilization [9,10]. These strategies include a coverage graft with organic molecules (surfactants or polymers) or coverage with an inorganic film (silica or carbon). It is important to note that, in many cases of protection, the shell does not only stabilize the nanoparticles: it may also be used for further functionalities (such as with other nanoparticles or different ligands, depending on the desired application) [1,11]. Along this vein, recent studies [12–14] have demonstrated the high affinity of ethylenediaminetetraacetic acid (EDTA) for iron oxide nanoparticles, which may improve colloidal dispersibility, decrease high surface energy, and consequently decrease the nanoparticles agglomeration.

The chelating potential of EDTA may be used to synthesize EDTA-

* Corresponding author.
E-mail address: aroldogm@fc.unesp.br (A.G. Magdalena).

https://doi.org/10.1016/j.jpcs.2017.10.002
Received 7 June 2017; Received in revised form 3 September 2017; Accepted 2 October 2017
Available online 3 October 2017

Table 1
Nomenclature of samples.

Sample	Name	Sample	Name
Fe_3O_4 25 °C; AMB.	NP25AMB	Fe_3O_4-EDTA-0.002 M 25 °C; AMB.	NP-L0.002M25AMB
Fe_3O_4 25 °C; N_2	NP25N2	Fe_3O_4-EDTA-0.002 M 25 °C; N_2	NP-L0.002M25N2
Fe_3O_4 90 °C; AMB.	NP90AMB	Fe_3O_4-EDTA-0.002 M 90 °C; AMB.	NP-L0.002M90AMB
Fe_3O_4 90 °C; N_2	NP90N2	Fe_3O_4-EDTA-0.002 M 90 °C; N_2	NP-L0.002M90N2
		Fe_3O_4-EDTA 0.02 M90 °C; N_2	NP-L0.02M90N2
		Fe_3O_4-EDTA 0.2 M 90 °C; N_2	NP-L0.2M90N2

functionalized Fe_3O_4 nanoparticles, which may be proved to be promising for studies on the adsorption of heavy metals due to the EDTA chelating cations, thus forming complexes with their structures [12,13].

The present contribution presents a study in the synthesis conditions and characterization of EDTA-functionalized Fe_3O_4 nanoparticles using the co-precipitation method of synthesis and changing the experimental conditions in order to carefully determine the importance of the experimental parameters in the synthesis of these compounds. The considered parameters were synthesis temperature (25 °C versus 90 °C), atmospheric conditions (presence versus absence of N_2), and EDTA concentration (0.2, 0.02, and 0.002 mol L^{-1}).

2. Experimental

The chemical reagents used for the synthesis of EDTA-functionalized Fe_3O_4 nanoparticles were iron (II) chloride tetrahydrate (Merck), iron (III) chloride hexahydrate (Aldrich), ammonium hydroxide ~ 28% (Synth), and EDTA (Synth).

The nanomaterials were synthesized by the co-precipitation method with some modifications [1,8,10,12,13]. Four syntheses were performed in the case of the Fe_3O_4 nanoparticles and another four ones were performed in the case of the Fe_3O_4-EDTA particles under the following four experimental conditions: (1) controlled synthesis temperature at 25 °C without inert atmosphere; (2) controlled synthesis temperature at 25 °C under nitrogen atmosphere; (3) controlled synthesis temperature at 90 °C under reflux and without inert atmosphere; and (4) controlled synthesis temperature at 90 °C under reflux and nitrogen atmosphere.

In the first step, Fe3O4 nanoparticles were synthesized using 100 mL of precursor solution containing 0.030 mol iron (III) chloride hexahydrate and 0.015 mol iron (II) chloride tetrahydrate, to which it was added 10 mL of ammonium hydroxide. This mixture was left under constant agitation for 1 h at the experimental temperature and atmospheric conditions in (1) to (4). The final precipitate was separated using a magnet and washed many times with distilled water and acetone.

In the second step, the EDTA-functionalized Fe_3O_4 nanoparticles were synthesized by using the same procedure used for the synthesis of the Fe_3O_4 nanoparticles. Then, it was added of 50 mL of a 0.002 mol L^{-1} EDTA solution soon after the ammonium hydroxide was added. Two additional Fe_3O_4-EDTA nanoparticle syntheses were performed using the experimental conditions in (4) in a similar procedure, but changing the EDTA concentration. In these changes, 50 mL solutions with 0.02 mol L^{-1} of EDTA or 0.2 mol L^{-1} of EDTA were used.

In Table 1 are presented the different synthesis prepared with the parameters evaluated. As an example, the sample NP25N2 and NP-L2mM25AMB represents NP – Fe_3O_4 nanoparticles; L – EDTA ligand; 0.002 mol L^{-1}, 0.02 mol L^{-1} or 0.2 mol L^{-1} – EDTA concentration; 25 or 90 – synthesis temperature in °C, and N_2 or AMB – atmospheric conditions (nitrogen atmosphere or without inert atmosphere conditions, respectively).

Nanoparticles samples were characterized based on the X-ray diffractometer patterns obtained from a Rigaku-Rint 2000 diffractometer with CuK_α radiation. Transmission electron microscopy (TEM) was performed using a Philips CM-200 instrument with a super twin a-lens. The FTIR spectrum was measured using a Vertex 70 spectrometer (Bruker instruments). The Zetasizer Nano ZS system (Malvern Instruments) was also used in the zeta potential measurements. Variations in pH were controlled using HCl/NaOH.

3. Results and discussion

Fig. 1 shows the X-ray diffractograms from different synthesis parameters for the Fe_3O_4 nanoparticles (Fig. 1-a) and the Fe_3O_4-EDTA nanoparticles (Fig. 1-b). These X-ray diffractograms show the crystallographic planes representing the diffraction of magnetite in all of the systems studied. The syntheses under ambient atmospheric conditions (NP25AMB, NO90AMB, and NP-L0.002M25AMB) produced a crystallographic plane representing magnetite (Fe_3O_4) and maghemite (γ-Fe_2O_3), a finding that indicates oxidation during synthesis. According to Gupta et al. [1], organic or inorganic molecules are typically used during the precipitation process to inhibit the oxidation of nanoparticles. The

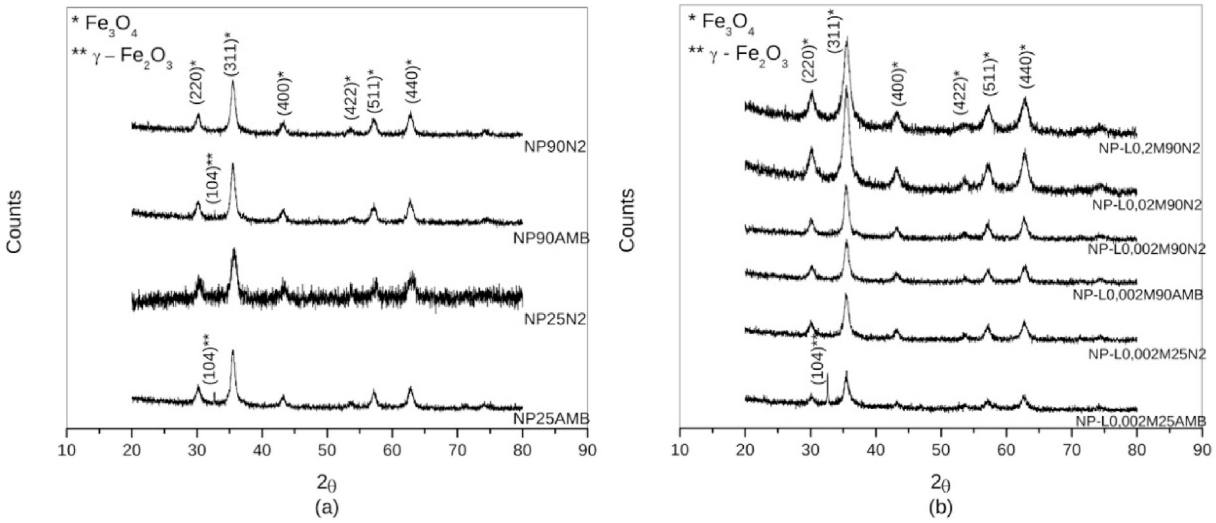

Fig. 1. X-ray diffraction patterns obtained for the samples. The magnetite (JCPDS card no. 89-0688) and maghemite (JCPDS card no. 89-0597) patterns from the JCPDS database.

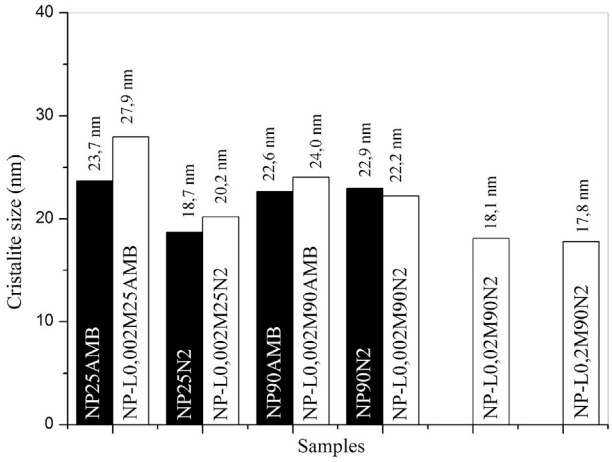

Fig. 2. Crystallite size obtained from the Scherrer equation to the samples.

magnetite (JCPDS card no. 89-0688) and maghemite (JCPDS card no. 89-0597) patterns from the JCPDS database for were included for comparison.

Even so, the oxidation of NP-L0.002M25AMB was found to occur in this experiment. However, in the case of NP-L0.002M90AMB and the other nanoparticles, the interaction was made by chemical binding between magnetite and EDTA molecules during synthesis. The EDTA molecules are attached in the nanoparticles. The EDTA-functionalized nanoparticles inhibits oxidation process of magnetite (Fe_3O_4) leading to maghemite (γ-Fe_2O_3). Kinetically controlled oxidation of ferrous species may be decreased through the use of a system to remove oxygen from the reaction medium. This may be obtained from the gas nitrogen streaming during the synthesis. The ideal molar reaction for the synthesis of magnetite is 2:1 ratio to Fe^{3+}:Fe^{2+}. To guarantee this ratio, inert atmosphere is used in the reaction medium. This control is very important: it may modify the surface properties of these materials, as well as the magnetic properties, which tend to decrease with oxidation.

As can be seen, temperature does not seem to significantly influence the stability of the phases. Iron oxide nanoparticles exhibited greater crystallinity in the samples synthesized at 90 °C than in those performed at 25 °C. Taking into account that for these systems, nucleation must occur before the growth of pre-formed nucleus, the temperature should favor the growth stage of the samples synthesized at 25 °C, thus increasing the diffusion of iron atoms to the nucleus that is formed. At this point, the dominant stage begins to occur as a growth mechanism, meaning that the speed of iron atom aggregation in the nanoparticles comes to depend on the quantity of these atoms around the nucleus.

The graph in Fig. 2 shows an estimate of the crystalline sizes obtained using the Scherrer equation [15]. In this work, the Scherrer's equation was used as the first approximation to determine the particle size, taking in consideration the uncertainty associated to this equation, as previously discussed by Tomaszewski [16]. Further up, the particles size were determined using the images obtained by TEM (Figs. 3-b, 4-b and 5), which is more appropriate to this purpose. The result indicates that all of the synthesized materials exhibit a nanometric particle size between 17.8 and 27.9 nm. The EDTA-functionalized Fe_3O_4 samples also exhibited smaller particle sizes. The use of nitrogen atmosphere prevented the oxidation process and aided in the control of particle size. All of the samples to which nitrogen gas streaming was applied were smaller than those in which ambient atmospheric conditions were used. This effect was found to be more pronounced at 25 °C. Because the growth process is favored at 90 °C, the crystallite sizes are very similar, a result that indicates that the expected findings involving temperature are consistent with the experimental data.

Fig. 2 also shows that the samplesNP-L0.002M90N2, NP-

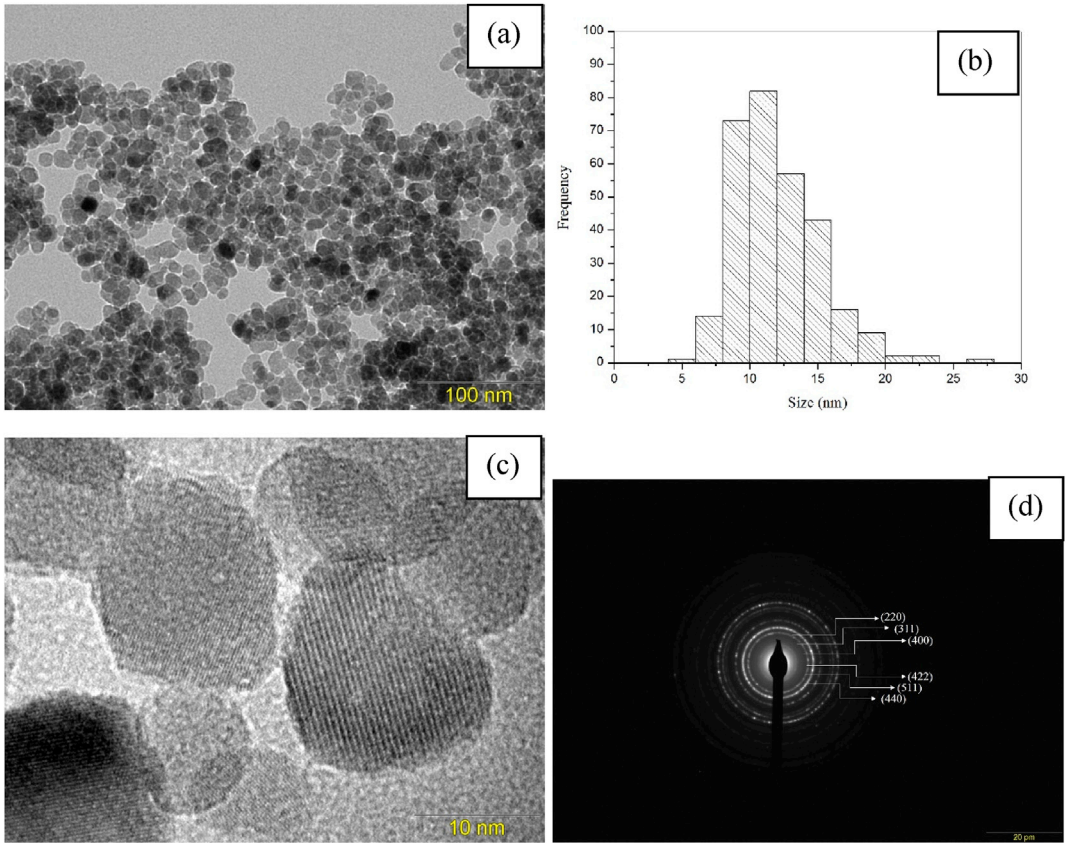

Fig. 3. Transmission electron microscopy for the nanoparticle referred to as NP90N2.

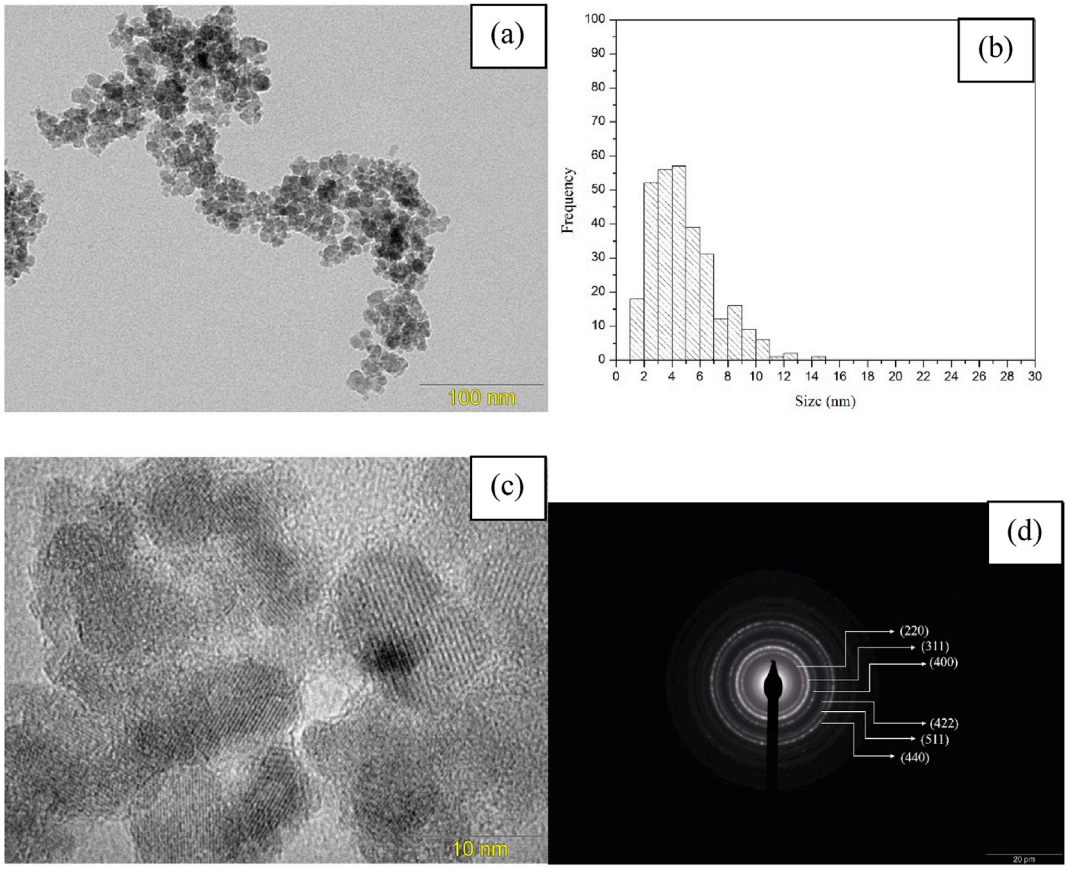

Fig. 4. Transmission electron microscopy for the nanoparticle referred to as NP-L0.2M90N2.

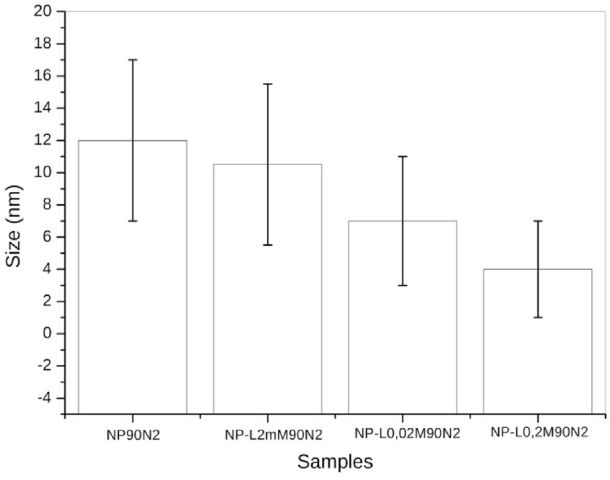

Fig. 5. Average size of some of the synthesized nanostructures.

L0.02M90N2, and NP-L0.2M90N2 nanostructures were found to be smaller in size than all of the other structures studied. As its concentrations increase, EDTA likely changes the mechanism of nanoparticle formation, which in turn, favors more nucleation than in the growth stage. In this case, EDTA is likely functioning as a barrier to the nuclei that are formed, resulting in decreased nanoparticle size.

The electron transmission micrographs in Figs. 3 and 4 shows that the nanostructures are highly homogeneous in shape and size. The micrographs (Fig. 3 and c) show that the average nanoparticle size was found to be approximately 12 nm in the case of NP90N2 nanoparticle, as verified in the histogram in Fig. 3-b. Similarly, the micrographs in Fig. 4a and c reflect the average size of 4 nm for the case of the NP-L0.2M90N2 nanoparticle, as presented in the histogram in Fig. 4c.

The transmission electron micrographs clearly show the crystallographic planes present in the nanostructures in Figs. 3c and 4c, and Figs. 3d and 4d represent the electron diffraction in these nanostructures. These results are consistent with the crystallographic planes presented in the X-ray diffraction patterns shown in Fig. 1.

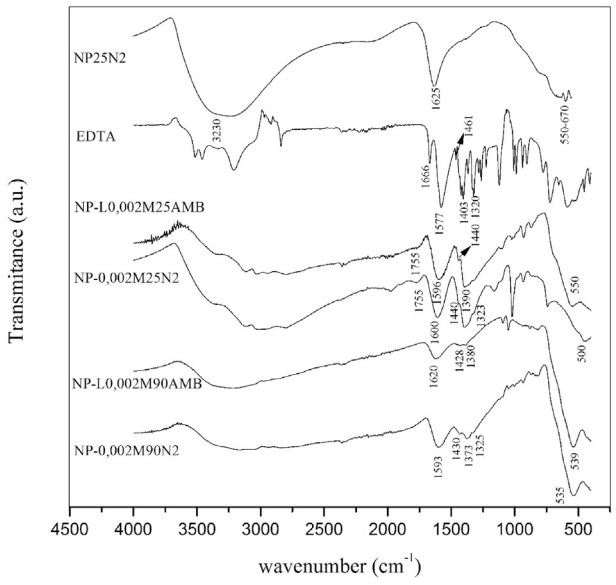

Fig. 6. Infrared spectra from investigated functionalized iron oxide nanoparticles. The main bands are featured.

Table 2
Description of the FTIR bands assignment of the spectra shown in Fig. 6.

NP25N2	EDTA	NP-L0.002M25AMB	NP-L0.002M25N2	NP-L0.002M90AMB	NP-L0.002M90N2
(550-670) Fe—O	–	(550) - Fe—O	(500) - Fe—O	(539) - Fe—O	(535) - Fe—O
–	(900-960) υ (C—C)	(870-930) υ (C—C)	(933) υ (C—C)	(880) υ (C—C)	(870-930) υ (C—C)
–	(1006) -υ [N (-CH_2—)$_3$]	(1020.1006 and 972) υ [N (-CH_2—)$_3$]	(1018 and 975) υ [N (-CH_2—)$_3$]	(1091.1048 and 975) υ [N (-CH_2—)$_3$]	(1044-1002) υ [N (-CH_2—)$_3$]
–	(1320) δ (NH^+)	(1325) δ (NH^+)	(1323) δ (NH^+)	–	(1325) δ (NH^+)
–	(1403) υ (C - O) COOH	(1390) υ (C - O) COOH	(1390) υ (C - O) COOH	(1382) υ (C - O) COOH	(1373) υ (C - O) COOH
–	(1461) υ_{si} (COO^-)	(1440) υ_{si} (COO^-)	(1440) υ_{si} (COO^-)	(1428) υ_{si} (COO^-)	(1430) υ_{si} (COO^-)
–	(1577) υ_{ass} (COO^-)	(1596) υ_{ass} (COO^-)	(1600) υ_{ass} (COO^-)	(1620) υ_{ass} (COO^-)	(1593) υ_{ass} (COO^-)
(1625) υ (H_2O)	–	–	–	–	–
–	(1666) υ (C = O) COOH	(1755) υ (C = O) COOH	(1774) υ (C = O) COOH	–	–
–	(2837-3210) υ (C -H)	(2800-3112) υ (C -H)	(2792-3119) υ (C -H)	–	(2844-3042) υ (C -H)
(3230) υ (O—H)	(3458-3512) υ (O—H)	(3340) υ (O—H)	(3362) υ (O—H)	(3221) υ (O—H)	(3200) υ (O—H)

The XRD and TEM results are in agreement with the reported data by Refs. [10,17]. Because in the homogeneous nucleation process there should be supersaturation of the precursors, that should be sufficient for the formation of the critical radius for the occurrence of the precipitate. Furthermore, the nanoparticles precipitate obtained shows high surface energy and elevated surface charge and tend to form agglomerates to minimize this surface energy, thus increasing the average size of the nanoparticles. To minimize the high values of surface energy, it commonly adds organic and/or inorganic molecules, which will interact with the nanoparticles to avoid the agglomerate and consequently allows the kinetic control of growth stage.

The graph in Fig. 5 shows the average sizes of the NP90N2, NP-L0.002 M 90N2, NP-L0.02M90N2, and NP-L0.2M90N2 nanostructures. The nanoparticle sizes were determined based on the histograms from the TEM analyses. The results confirm the proposal that the addition of EDTA will favor the nucleation stage of the nanoparticles. The graph in Fig. 5 also shows the influence of EDTA concentration on particle size: the results reflect the decrease in nanoparticle size as EDTA concentration increased, which is consistent with the results provided by the use of the X-ray diffraction technique.

In order to confirm the functionalization of EDTA on the surface of the nanoparticles, infrared spectroscopy analyses were performed and the resulting graphs are shown in Fig. 6.

In the infrared spectrum of magnetite (NP25N2) shown in Fig. 6, three bands are visible: the first one is found between 560 and 670 cm^{-1} and is assigned to the binding of iron to oxygen, a property required for the formation of Fe_3O_4; the second band is found near 1625 cm^{-1} and is the result of the absorption of water molecules; and the third band, found near 3230 cm^{-1}, is associated with stretching υ (O—H). The latter band proves the formation of hydroxyl groups on the surface of magnetite. Fig. 6 also allows for an analysis of the pure EDTA spectrum, on which a series of bands were found. Bands were found at 900-960 cm^{-1} due to the ν(C—C) axial deformations, at 1006 cm^{-1} due to the asymmetrical axial deformations in the group ν [N (-CH_2—)$_3$] of the tertiary amines, at 1320 cm^{-1}, which is attributed to angular deformation δ (NH^+), near 1461 and 1577 cm^{-1}, which is attributed to symmetrical and asymmetrical axial deformation ν (COO^-), and between 1403 and 1666 cm^{-1}, which corresponds to vibrational motions ν(C—O) and ν(C═O) of the —COOH group. There were also many bands between 2837 and 3210 cm^{-1}, which were associated with the ν(C—H) axial deformities of the CH_2 groups. Finally, the bands between 3458 and 3512 cm^{-1} are attributed to stretching υ (O—H) resulting from water and hydration in this compound. Table 2 contains all of the bands found for each of the samples analyzed.

Infrared spectra attributed to the functionalization of the EDTA on the surface of Fe_3O_4 nanoparticles are the in Fig. 6 (NP-L2mM25AMB, NP-L2mM25N2, NP-L2mM90AMB, and NP-L2mM90N2). FTIR spectra for the NP-L0.02M90N2 and NP-L0,2M90N2 samples are very similar to those of the NP-L0.002M90N2 nanoparticles. The appearance of new FTIR bands for pure magnetite can also be seen and they are attributed to the functionalized EDTA molecule on the magnetic nanoparticles surface. Another remarked aspect of these graphs is the decrease in band intensity associated to the stretching υ (O—H) to approximately 3230 cm^{-1}. This result indicates that, in cases of functionalization with EDTA, these groups are recovered and/or are participating in chemical reactions. Another finding is that magnetite may bind with the carboxylates of EDTA, since the carboxylates exhibit considerable distortion in the ν (C—O) and stretching υ_{ass} (COO^{-1}) bands of pure EDTA, a result which

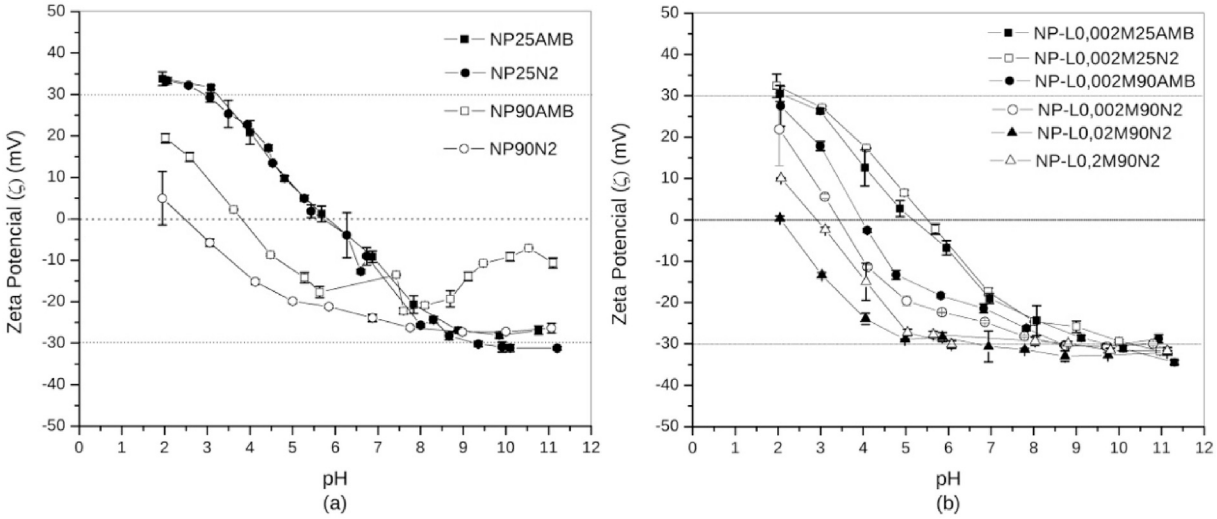

Fig. 7. Zeta potential measurements as a function of pH for (a) Fe_3O_4 nanoparticles and (b) EDTA-functionalized Fe_3O_4 nanoparticles.

indicates that the EDTA binds on the surface of nanoparticles at these sites [11,12,14].

The FTIR results showed that occurred the EDTA functionalization in all samples of magnetite. Already Yang et al. [13] synthesized the Fe_3O_4-EDTA nanoparticles by the coprecipitation method keeping the product at 90 °C for 30 min. The EDTA functionalization shows that the EDTA exhibits high chemical affinity for Fe_3O_4 nanoparticles, even at room temperature. Moreover, the EDTA addition should be a cheap and satisfactory alternative for protection and functionalization of nanostructures. This system shows high potential to metal [12] and anions [13] adsorption. The FTIR spectra also show that the interaction between EDTA and magnetite occurs by the carboxylate anion. This result enables future functionalizations, since there is another carboxylate group in addition to tertiary nitrogens.

Fig. 7 shows the zeta potential curves (ζ) as a function of pH for the Fe_3O_4 nanoparticles (Fig. 7a) and for the Fe_3O_4–EDTA nanoparticles (Fig. 7b). In the case of the naked Fe_3O_4 nanoparticles, the zeta potential was found to be more influenced by the synthesis temperature than by atmospheric conditions. This result is reflected in the graph showing crystallite size as evaluated by the Scherrer equation (Fig. 2), in which the nanostructures exposed to the higher temperature (90 °C in the nitrogen atmosphere) increased slightly in size. This increase led to greater colloidal instability in these samples, and changes in the isoelectric point to lower pH values were found in the samples synthesized at 90 °C. In the case of the EDTA-functionalized Fe_3O_4 nanoparticles, behavior similar to that which was observed in the Fe_3O_4 nanoparticles was seen in the samples synthesized at 25 °C. Increased isoelectric points were found among the samples synthesized at 90 °C.

These results show that the charge density associated with the EDTA carboxyl group is predominant, and they are consistent with the results indicated by the IR spectroscopy. The analysis involving the concentration of EDTA (NP-L0.2M90N2 and NP-L0.02M90N2) found low isoelectric points due to high surface energy caused by the reduction in size, which changed the distribution of charges on the surface of the nanoparticles. These results are very promising for environmental remediation applications in the adsorption of heavy metals on the nanoparticles surface.

4. Conclusions

The results show that, in synthesis, the inert atmosphere associated with the co-precipitation method is fundamental for preventing the oxidation of magnetite. Furthermore, the X-ray diffraction analyses determined that temperature influences crystalline size, since the growth stage is favored at higher temperatures. The results reflect high homogeneity in nanoparticle shape and size in the samples studied. The addition of EDTA was also found to act as a barrier to the growth of nanoparticle nuclei, thus decreasing nanoparticle size. The functionalization of the surface of magnetite was confirmed by the Fourier transform infrared (FTIR) spectroscopy analyses and the development of new bands associated with EDTA. The zeta potential measurements showed that the distribution of charges on the surface of the samples is affected by synthesis temperatures and EDTA concentrations.

Acknowledgements

The authors are grateful for the support from the Institutional Scientific Research Grant Program of São Paulo State University (PROPe/UNESP) - First Project Grant Request No. 775.

References

[1] A.K. Gupta, M. Gupta, Synthesis and surface engineering of iron nanoparticles for biomedical applications, Biomaterials 26 (2005) 3995–4021.
[2] J. Yang, S.B. Park, H.G. Yooh, Y.M. Huh, S. Haam, Preparation of poly ε-caprolactone nanoparticles containing magnetite for magnetic drug carrier, Int. J. Pharm. 324 (2006) 185–190.
[3] Z. Wang, R. Qiao, Na Tanga, Z. Lud, H. Wanga, Z. Zhange, X. Xuef, Z. Huangf, S. Zhangf, G. Zhanga, Y. Lif, Active targeting theranostic iron oxide nanoparticles for MRI and magnetic resonance-guided focused ultrasound ablation of lung cancer, Biomaterials 127 (2017) 25–35.
[4] G.S. Parkinson, Iron oxide surfaces, Surf. Sci. Rep. 71 (2016) 272–365.
[5] A. Akbarzadeh, M. Samiei, S. Davaran, Magnetic nanoparticles: preparation, physical properties, and applications in biomedicine, Nanoscale Res. Lett. 7 (2012) 144–157.
[6] R.M. Comell, U. Schwertmann, The Iron Oxides – Structure, Properties, Reactions, Occurences and Uses, second ed., Wiley-VCH Verlag GmbH & Co. KGaA, Weinheim, 2003.
[7] S.C.N. Tang, I.M.C. Lo, Magnetic nanoparticle: essential factors for sustainable environmental applications, Water Res. 47 (2013) 2613–2632.
[8] R. Bini, R.F.C. Marques, F.J. Santos, J.A. Chaker, M. Jafelicci Jr., Synthesis and functionalization of magnetite nanoparticles with different alkoxysilanes, J. Magn. Magn. Mater 324 (2012) 534–539.
[9] An-Hui Lu, E.L. Salabas, F.S. Schüth, Magnetic nanoparticles: syntesis, protection, functionalization, and application, Angew. Chem. Int. Ed. 46 (2007) 1222–1244.
[10] S. Laurent, D. Forge, M. Port, et al., Magnetic iron oxide nanoparticles: synthesis, stabilization, Vvectorization, physicochemical characterizations, and biological applications, Chem. Rev. 108 (2008) 2064–2110.
[11] R.J. Hunter, Introduction to Modern Colloid Science, Oxford University Press, New York, 1993.
[12] C.L. Warner, R.S. Addleman, A.D. Cinson, et al., High-Performance, superparamagnetic, nanoparticle-based heavy metals sorbents for removal of contaminants from natural Waters, ChemSusChem 3 (2010) 749–757.
[13] J. Yang, Q. Zeng, L. Peng, et al., La-EDTA coated Fe_3O_4 nanomaterial: preparation and application in removal of fosfate from water, J. Environ. Sci. 25 (2013) 413–418.
[14] K. Azizi, E. Ghonchepour, M. Karimi, A. Heydari, Encapsulation of Pd (II) into superparamagnetic nanoparticles grafted with EDTA and their catalytic activity towards reduction of nitroarenes and Suzuki-Miyaura coupling, Appl. Organomet. Chem. 29 (2015) 187–194.
[15] B.D. Cullity, Elements of X-Ray Diffraction. 2nd ED., London, 1977, p. 411.
[16] P.E. Tomaszewski, The uncertainly in grain size calculation from X-ray diffraction data, Phase Transitions 83 (2013) 260–266.
[17] M.A. Martins, T. Trindade, Os nanomateriais e a descoberta de novos mundos na bancada do químico, Quim. Nova 35 (2012) 1434–1446.